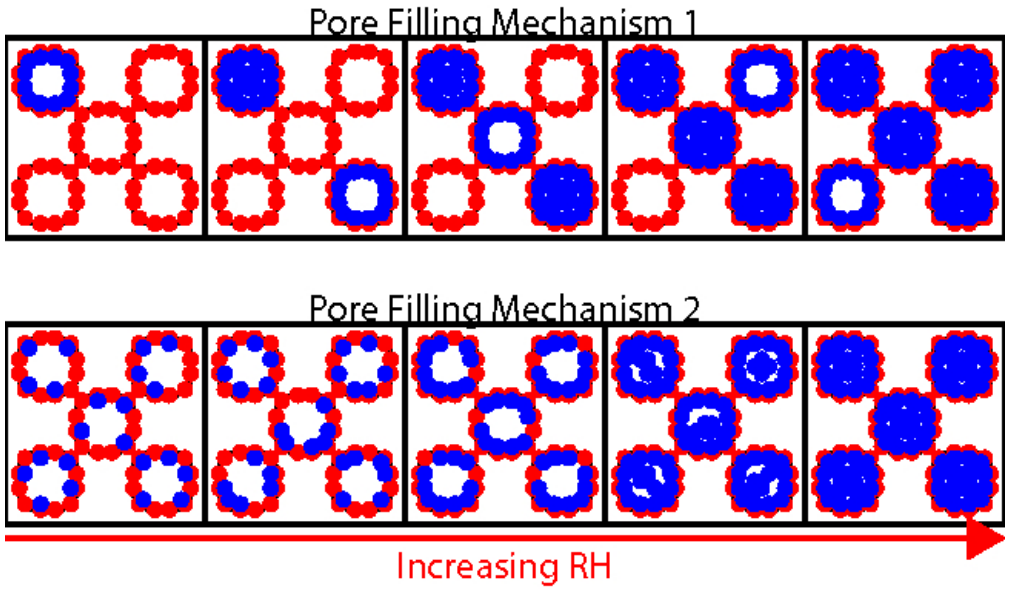

Figure 1. Proposed layer/cluster mechanism. In mechanism 1, individual pores are filled before additional pores are filled, while in mechanism 2, all pores fill simultaneously at a similar rate.

82x48mm (200 x 200 DPI)

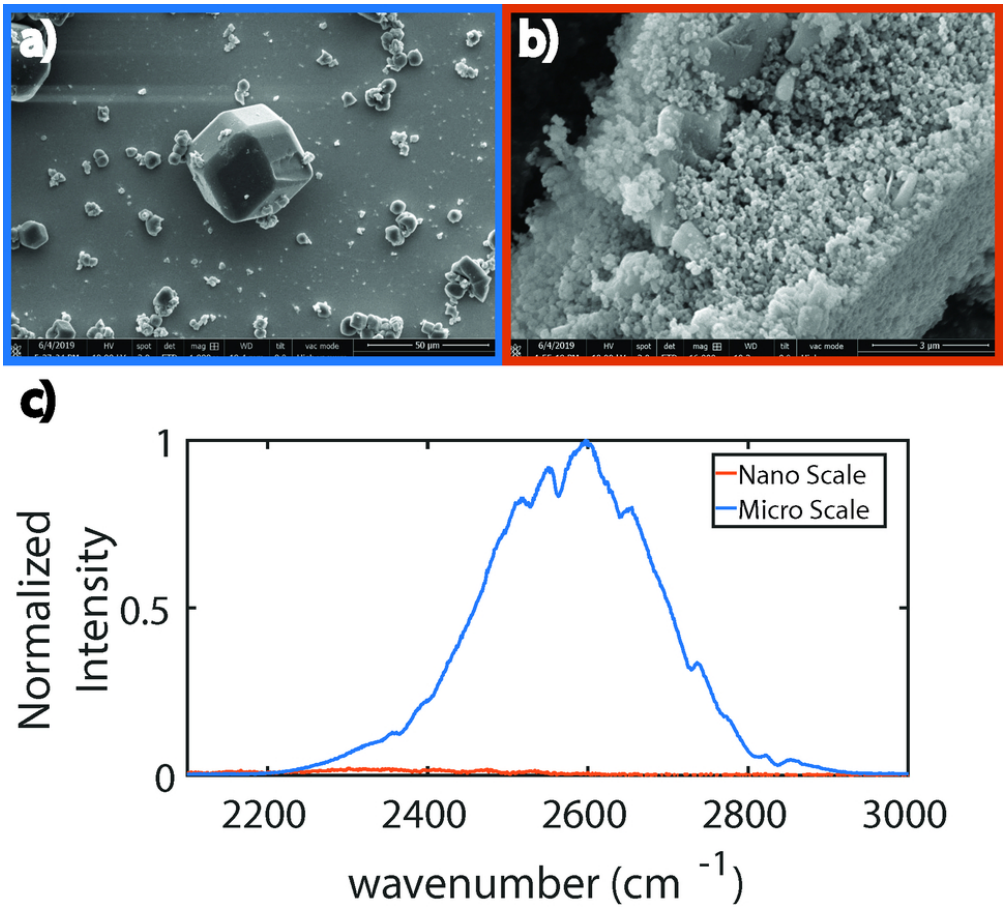

Figure 2. SEM images a) micron-sized and b) nanometer-sized ZIF-90 crystals. The corresponding SFG signal is large for the micron-sized crystal but negligible for the nanocrystals.

81x73mm (300 x 300 DPI)

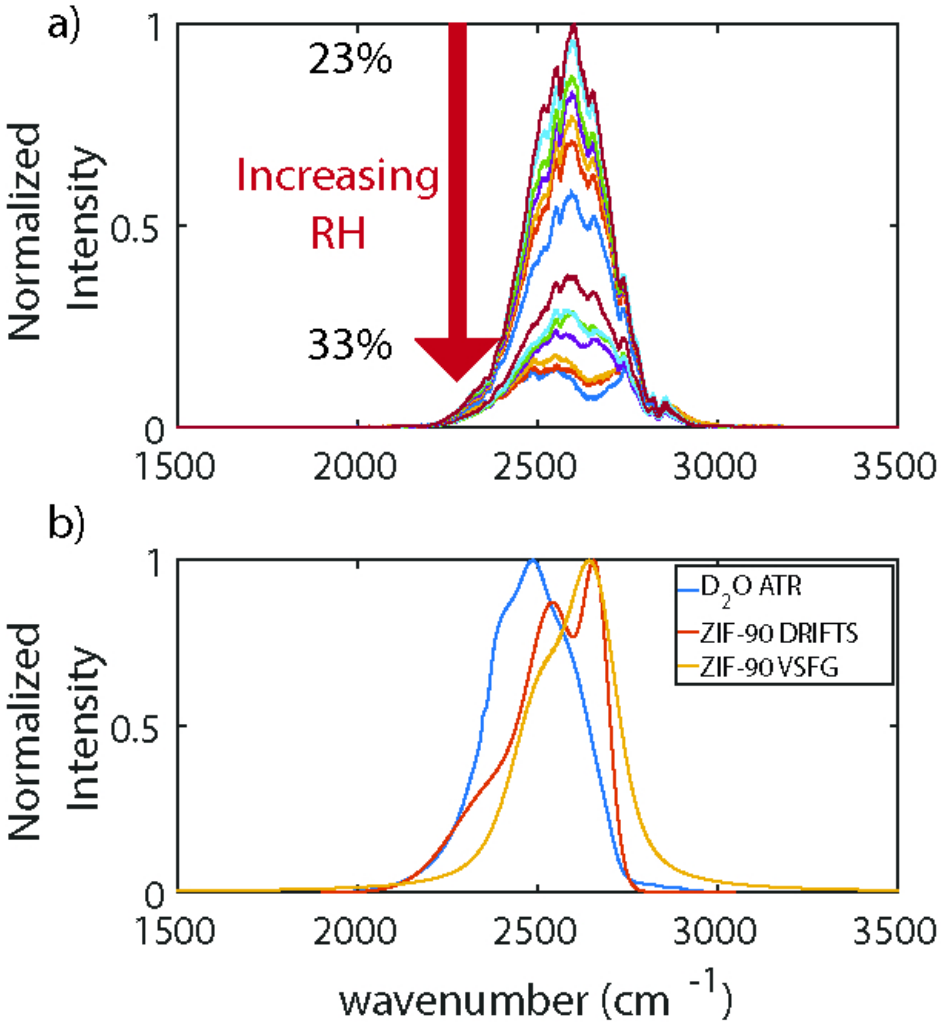

Figure 3. a) Raw VSFG spectra from 23% to 33% RH, b) an ATR spectrum of pure bulk heavy water, a DRIFTS spectrum at 43% RH and an extracted VSFG spectra at 33% RH of heavy water adsorbed by ZIF-90.

82x85mm (200 x 200 DPI)

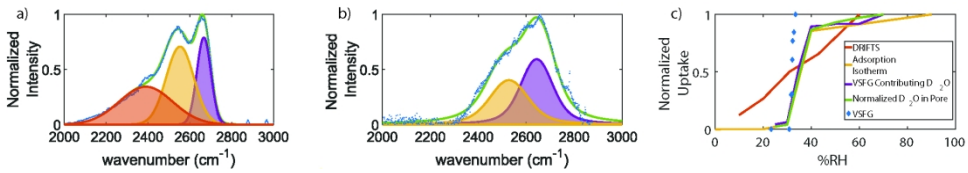

Figure 4. a) Fitting results for DRIFTS at 43% RH purge. b) VSFG at 33.4% fitting results c) VSFG integrated spectral intensity (blue), DRIFTS 2665 cm-1 peak (red), adsorption isotherm (yellow), bound heavy water that contribute to VSFG signal (purple), and total simulated heavy water in the pores versus RH (green).

266x44mm (200 x 200 DPI)

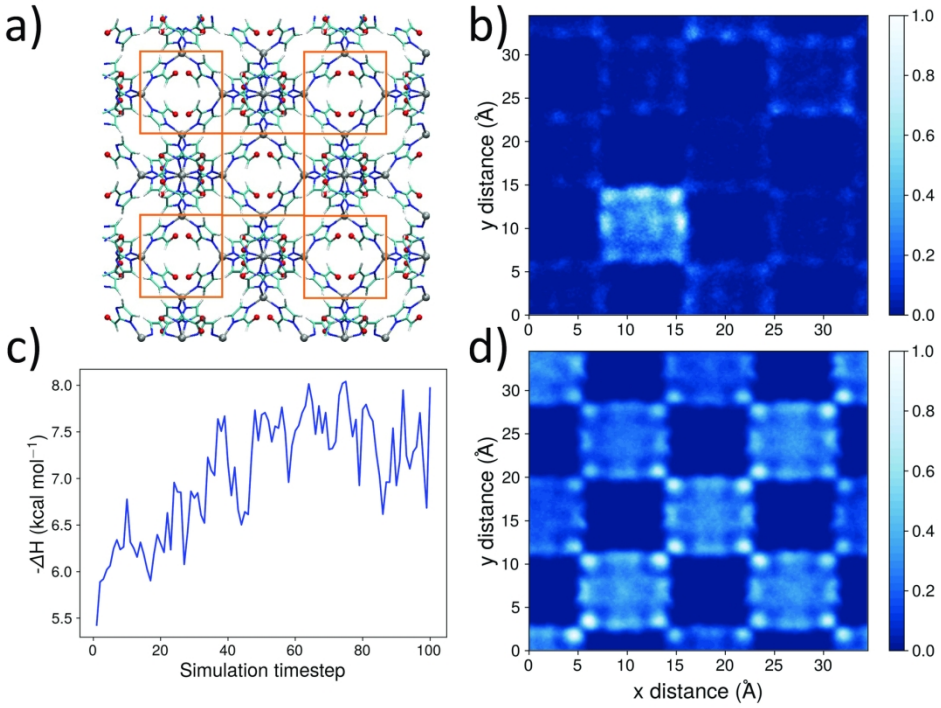

Figure 5. MD simulations to show the water molecule distri-bution as a function of RH. (a) Schematic of the ZIF-90 framework used in the simulation, each square indicates pore space where water can be adsorbed. (b) at 30% RH, water preferentially clusters in single unit cells, and only the sur-face site on this specific unit cells are occupied, whereas (c) at 40% RH, water evenly distributes among unit cells with all surface site occupied. (d) The enthalpy of adsorption at 30% RH of water in ZIF-90 shows that when starting with water evenly distributed in the materials, its enthalpy of adsorption increases by clustering into single unit cells.

82x59mm (600 x 600 DPI)

Water Capture Mechanisms at Zeolitic Imidazolate Framework Interfaces

Jackson C. Wagner[1], Kelly M. Hunter[1], Francesco Paesani[1,2]*, Wei Xiong[1,2,3]*

[1]Department of Chemistry and Biochemistry, University of California, San Diego, CA, USA, 92093

[2]Materials Science and Engineering Program, University of California, San Diego, CA, USA, 92093

[3]Department of Electrical and Computer Engineering, University of California, San Diego, CA, USA, 92093

ABSTRACT: Water capture mechanisms of zeolitic imidazolate framework ZIF-90 are revealed by differentiating the water clustering at interior interfaces of ZIF-90 and the center pore filling step, using vibrational sum-frequency generation spectroscopy (VSFG) at a one-micron spatial resolution. Spectral lineshapes of VSFG and IR spectra suggest that OD modes of heavy water in both water clustering and center pore filling steps experience similar environments, which is unexpected as weaker hydrogen bond interactions are involved in initial water clustering at interior surfaces. VSFG intensity shows similar dependence on the relative humidity as the adsorption isotherm, suggesting that water clustering and pore filling occur simultaneously. MD simulations based on MB-pol corroborate the experimental observations, indicating that water clustering and center pore filling happen nearly simultaneously within each pore, with water filling the other pores sequentially. The integration of nonlinear optics with computational simulations provides critical mechanistic insights into the pore filling mechanism that could be applied to the rational design of future MOFs.

Interest in atmospheric water capture materials has grown recently as the supply of fresh water becomes scarce. Metal-organic frameworks (MOFs), a class of porous crystalline solids composed of transition metal centers coordinated to organic linkers, hold great promise for water harvesting purposes due to their high porosity and tunability. Understanding the water capture mechanisms, which depend on the competition between water-framework and water-water interactions, is crucial to rationally designing MOFs for energy-efficient water capture.[1–4]

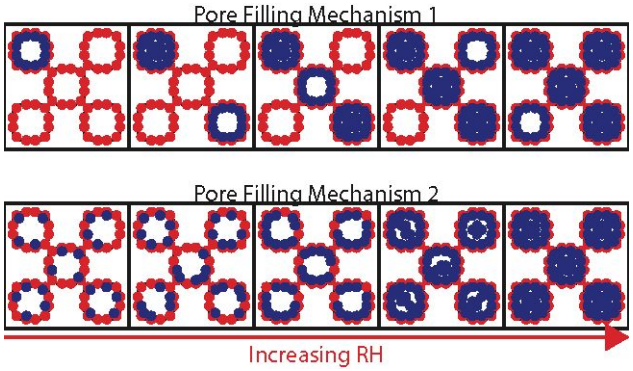

Figure 1. Proposed layer/cluster mechanism. In mechanism 1, individual pores are filled before additional pores are filled, while in mechanism 2, all pores fill simultaneously at a similar rate.

Among different water adsorption mechanisms in MOFs,[1–3] the layer/cluster adsorption is a common mechanism in which water clusters are firstly formed through nucleation on hydrophilic sites in the MOF. Then, water uptake at the center of the pore occurs through reversible pore filling.[2] While the mechanistic step is clear, specific details are missing.[5,6] For example, water clustering and center pore filling could occur sequentially on single pore levels, but simultaneously overall (Mechanism 1, Fig. 1). Alternatively, water clusters could form in every pore at a certain relative humidity (RH) and, after all pores have water clusters near the hydrophilic sites, center pore filling starts (Mechanism 2, Fig. 1).

The lack of mechanistic detail is largely due to the difficulty in separately probing water clustering and pore filling. The initial water cluster formation happens at the interior surface of MOFs, which requires interfacial specific techniques to probe. Common methods to study MOFs, such as adsorption/desorption isotherms,[7–9] only report the number of water molecules in the pores. Diffuse reflectance infrared Fourier transform spectroscopy (DRIFTS) can only probe the molecular details of bulk water adsorption in MOFs.[10,11] Although several studies using diffraction techniques have revealed molecular-level details of water adsorption in a few MOFs, its application for the pore filling mechanism has been limited.[12–14] On the other hand, molecular dynamics (MD) simulations can provide molecular-level insights into interfacial processes, but these simulations often lack corresponding experimental comparison.[10,11,15–17]

In this work, we reveal that the adsorption mechanisms of water in ZIF-90 mechanism 1. This work is feasible by selectively probing the water clustering step, using a spatially-resolved vibrational sum-frequency generation (VSFG) spectroscopy and MB-pol[18–20] water-based simulations.[11] This study emphasizes the importance of interfacial-specific techniques[21–26] to decipher the effects of

water-water and water-framework interactions on the water adsorption mechanism, which can provide guidance to the rational design of MOFs for water harvesting.

Two crucial technical aspects that enable the micron-resolved VSFG to probe adsorbed water at interior MOF surfaces. First, ZIF-90 lacks inversion symmetry which ($I\bar{4}3m$ space group) makes it VSFG active. Indeed, the metal center in ZIF-90 (under dry conditions) even generates a strong second order non-resonant background signal (broad feature at 2500 cm^{-1}) [27]. The interactions between water and the organic linkers template the water hydrogen-bond network that adopts the same symmetry as ZIF-90, becoming VSFG active. [28–34] Because VSFG probes water adsorbed on hydrophilic groups that compose the interior interfaces, it is sensitive to the initial water cluster formation stage.

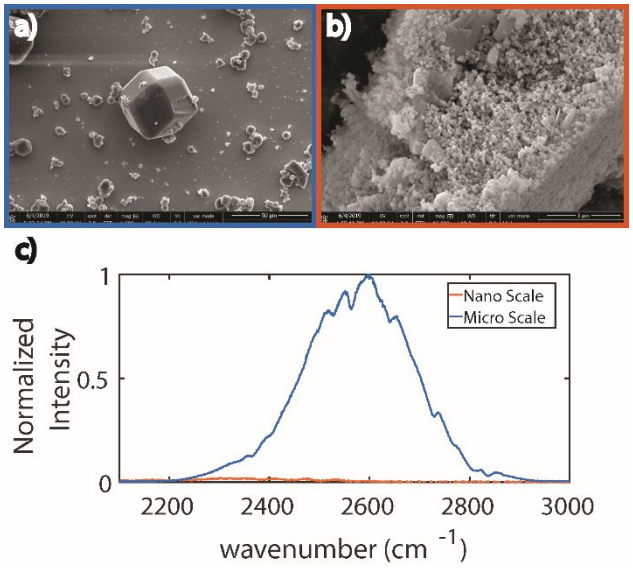

Figure 2. SEM images a) micron-sized and b) nanometer-sized ZIF-90 crystals. The corresponding SFG signal is large for the micron-sized cyrstal but neglegible for the nanocrystals.

Second, although individual ZIF-90 crystals are VSFG active, signals from a collection of randomly oriented ZIF-90 crystals cancel each other. We deployed the VSFG microscope to resolve single microcrystals at c.a. 1μm resolution.[35] The necessity of this effort is evident by the comparison of the signal from ZIF-90 with 10s of microns diameters (sample A, Fig. 2a), and the signal from aggregates of nanocrystals (sample B, Fig. 2b). While other characterizations indicate both materials are ZIF-90 (SI Fig 3), only sample A has strong VSFG signal (Fig. 2c). The microscope (1.6 micron resolution) thus can resolve the individual facets of single crystals in sample A, but not the randomly packed nanocrystals in sample B. Similar averaging would occur to sample A if a VSFG spectrometer with >100 micron beam diameter were used.[36] In the following, we only focus on studying water adsorption in sample A.

Upon D_2O adsorption of ZIF-90, spectral signatures appear. As the RH is increased from 23% to 29%, a reduction in the overall non-resonant signal appears, possibly due to changes in refractive indices upon external water condensation. A new dip appears and becomes apparent at 31% RH (Fig. 3a). This feature appears exclusively during D_2O adsorption. Combined with its center frequency, it is assigned to the OD stretch of adsorbed D_2O on the ZIF-90 interior surface, due to the symmetry transfer from ZIF-90. Other possible origins of such a spectral change[37] were examined and ruled out (SI Fig 5 and 6 for details).

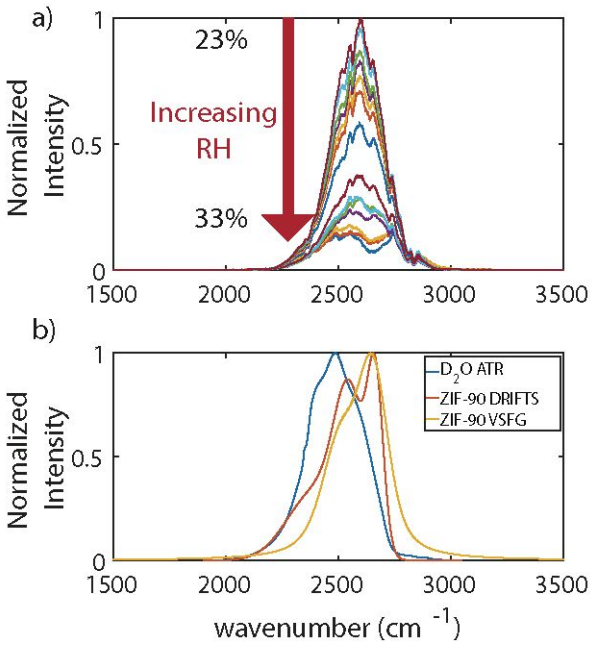

Figure 3. a) Raw VSFG spectra from 23% to 33% RH, b) an ATR spectrum of pure bulk heavy water, a DRIFTS spectrum at 43% RH and an extracted VSFG spectra at 33% RH of heavy water adsorbed by ZIF-90.

We extract the OD feature by treating the non-resonant signal as a local oscillator (see SI S4 and SI Fig 8 for details). Compared to bulk D_2O, both the bulk (DRIFTS) and interfacial OD features of D_2O in ZIF-90 exhibit blueshifts (Fig. 3b), suggesting weaker hydrogen bond interactions experienced by the D_2O molecules in ZIF-90. Our previous results from MD simulations agree with this observation.[11]

To quantitatively analyze the spectra, we fit DRIFTS and VSFG spectra (SI Fig 7 and 9). The DRIFTS spectra are fit with three gaussian peaks at 2400 cm^{-1}, 2550 cm^{-1} and 2665 cm^{-1} (Fig. 4a), while VSFG spectra are fit with two peaks centered at ~2515 cm^{-1} and 2630 cm^{-1} (Fig. 4b). Besides the Fermi resonance at 2400 cm^{-1}, the 2550 cm^{-1} and 2665 cm^{-1} peaks were assigned to the asymmetric and symmetric OD stretching modes, based on results from MB-pol simulations.[11] We note for DRIFTS, the two modes' intensities are comparable, while in VSFG, the symmetric mode is more intense. This difference possibly arises because DRIFTS only depends on the transition dipole moment, whereas VSFG is proportional to both transition dipole and polarizability. The difference in peak intensities and missing of Fermi resonance in VSFG also suggest that the VSFG signal is not a phantom signal due to liquid water absorption.[37] The fact that the peaks in both DRIFTS and VSFG spectra have similar spectral position is counterintuitive. As explained above, VSFG probes D_2O

bound to the hydrophilic linker at the step of water clustering, whereas DRIFTS probes all D_2O inside the pore, at both water clustering and pore filling steps. Since hydrogen bonding between D_2O and organic linkers is weaker than that between D_2O molecules,[11] we expect the VSFG spectra to be more blue-shifted relative to the DRIFTS

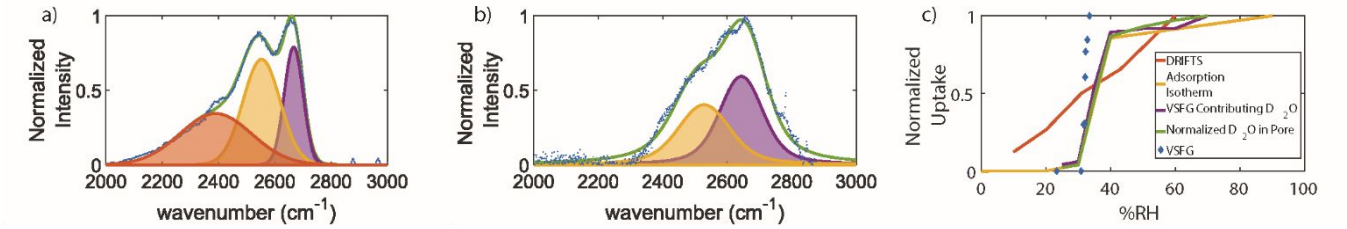

Figure 4. a) Fitting results for DRIFTS at 43% RH purge. b) VSFG at 33.4% fitting results c) VSFG integrated spectral intensity (blue), DRIFTS 2665 cm^{-1} peak (red), adsorption isotherm (yellow), bound heavy water that contribute to VSFG signal (purple), and total simulated heavy water in the pores versus RH (green).

spectra. Similar spectral positions in DRIFTS and VSFG seem to suggest that D_2O molecules in the water clustering and pore filling steps experience similar local environments. A more unexpected result is that the peak intensities of DRIFTS and VSFG show drastically different RH dependence (Fig. 4c). DRIFTS intensity increases steadily versus RH while VSFG spectra show a sharp increase near 30% of RH.

The DRIFTS trend indicates that there could be condensation prior to adsorption on the exterior of ZIF-90, which causes the steady increase in DRIFTS and, possibly, the decrease of the non-resonant SFG signal. The trend observed in the VSFG data is like the adsorption isotherm, however, more puzzling. Since VSFG probes D_2O bound to the interior surfaces of MOFs, it is expected that VSFG should be sensitive to the D_2O adsorption at early stages of hydration before the pore filling step occurs, which causes the step increase in the adsorption isotherm. In other words, the RH dependence of the VSFG signal suggests that water clustering and pore filling occur simultaneously.

MD simulations with MB-pol can shed light on the underlying molecular mechanisms. At 30% RH, the simulations indicate that instead of an even distribution across all pores of the simulation box, the D_2O molecules condense into a single pore. It is only at 40% RH, when nearly all pores are filled, that their interior surfaces are adsorbed by D_2O molecules (Fig. 5). This result is robust against the initial distribution of D_2O molecules (see SI S6 and SI Figs.10 and 11 for details).

We further plot the number of D_2O molecules adsorbed at interior surfaces, which can contribute to the VSFG signal, as well as the total number of adsorbed D_2O molecules as a function of RH (Fig. 4c, SI S6 for details), to determine if water clustering and pore filling occur concurrently (mechanism 1) or sequentially (mechanism 2). The number of D_2O molecules at the interior surface and the total number of D_2O molecules follow a similar trend and saturate at 40% when all pores are filled, which implies that water clustering and pore filling occur concurrently, with the D_2O molecules filling one pore after another, as in mechanism 1 (Fig. 1).

Our simulations further indicate that condensation in a single pore is energetically favorable. When water is clustered in a single pore, its enthalpy of adsorption is ~2 kcal/mol lower than when the D_2O molecules are evenly distributed (Fig.5c and SI Fig.12). This result agrees with our understanding water-carbonyl interactions being weaker than water-water interactions in ZIF-90. it is thus reasonable to expect that as water molecules adsorb onto the interior surfaces of ZIF-90, they serve as a seed to attract more water molecules. These additional water molecules prefer to hydrogen bond with the adsorbed water molecules, instead of binding to other aldehyde groups in other pores.

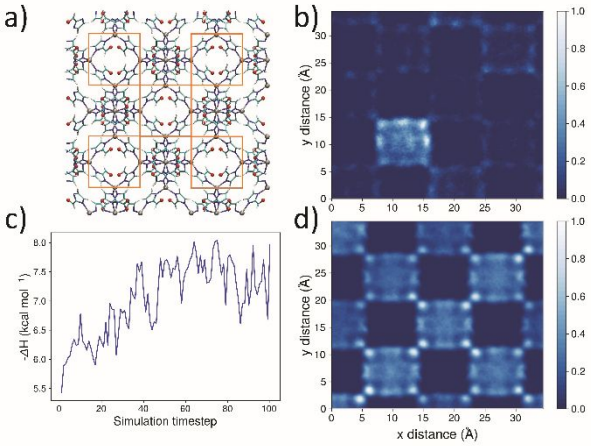

Figure 5. MD simulations to show the water molecule distribution as a function of RH. (a) Schematic of the ZIF-90 framework used in the simulation, each square indicates pore space where water can be adsorbed. (b) at 30% RH, water preferentially clusters in single unit cells, and only the surface site on this specific unit cells are occupied, whereas (c) at 40% RH, water evenly distributes among unit cells with all surface site occupied. (d) The enthalpy of adsorption at 30% RH of water in ZIF-90 shows that when starting with water evenly distributed in the materials, its enthalpy of adsorption increases by clustering into single unit cells.

The water pore filling mechanism also explains why the positions of the D_2O features in the DRIFTS and VSFG spectra are similar. Because water clustering and pore filling occur simultaneously, although the VSFG signal detects D_2O involved in the clustering step, these molecules experience hydrogen-bonding interactions with other D_2O molecules in the bulk. Therefore, the VSFG OD spectra have similar peak positions as bulk D_2O probed by DRIFTS, which is supported by the calculated density-of-state spectra of

bulk D_2O and D_2O adsorbed at the interior ZIF-90 surfaces (SI Fig 12).

The new ability of probing water cluster at interior surface of ZIF-90, integrated with MB-pol simulations suggest that water clustering and pore filling occur in single pores before water occupies other pores, driven by the stronger water-water interactions than water-framework interactions. The demonstrated method to probe the water clustering step can be applied to other MOFs to aid the optimization of water interactions and water capturing mechanisms.

ASSOCIATED CONTENT

SUPPLEMENTARY INFORMATION

This material is available free of charge via the Internet at http://pubs.acs.org

AUTHOR INFORMATION

Corresponding Author

* Francesco Paesani, fpaesani@ucsd.edu
* Wei Xiong, w2xiong@ucsd.edu

Author Contributions

The manuscript was written through contributions of all authors. All authors have given approval to the final version of the manuscript.

Funding Sources

This work is supported by Department of Energy, Basic Energy Science (BES) Office, Condensed Phase and Interfacial Molecular Science (CPIMS) Program (Award No. DE-SC0019333)

Notes

The authors declare no competing financial interests.

ACKNOWLEDGMENT

We would like to acknowledge Mark Kalaj from Dr. Seth Cohen for synthesizing ZIF-90 MOF. SEM imaging was done in part at San Diego Nanotechnology Infrastructure (SDNI) of UCSD, an NSF designated National Nanotechnology Coordinated Infrastructure site, supported by NSF grant ECCS-1542148.

REFERENCES

(1) Hanikel, N.; Prévot, M. S.; Yaghi, O. M. MOF Water Harvesters. *Nat. Nanotechnol.* **2020**, *15* (5), 348–355. https://doi.org/10.1038/s41565-020-0673-x.

(2) Canivet, J.; Fateeva, A.; Guo, Y.; Coasne, B.; Farrusseng, D. Water Adsorption in MOFs: Fundamentals and Applications. *Chem. Soc. Rev.* **2014**, *43* (16), 5594–5617. https://doi.org/10.1039/c4cs00078a.

(3) Liu, X.; Wang, X.; Kapteijn, F. Water and Metal-Organic Frameworks: From Interaction toward Utilization. *Chem. Rev.* **2020**, *120* (16), 8303–8377. https://doi.org/10.1021/acs.chemrev.9b00746.

(4) Yu, M. H.; Liu, X. T.; Space, B.; Chang, Z.; Bu, X. H. Metal-Organic Materials with Triazine-Based Ligands: From Structures to Properties and Applications. *Coord. Chem. Rev.* **2021**, *427*, 213518. https://doi.org/10.1016/j.ccr.2020.213518.

(5) Bon, V.; Senkovska, I.; Evans, J. D.; Wöllner, M.; Hölzel, M.; Kaskel, S. Insights into the Water Adsorption Mechanism in the Chemically Stable Zirconium-Based MOF DUT-67-a Prospective Material for Adsorption-Driven Heat Transformations. *J. Mater. Chem. A* **2019**, *7* (20), 12681–12690. https://doi.org/10.1039/c9ta00825j.

(6) Nandi, S.; Aggarwal, H.; Wahiduzzaman, M.; Belmabkhout, Y.; Maurin, G.; Eddaoudi, M.; Devautour-Vinot, S. Revisiting the Water Sorption Isotherm of MOF Using Electrical Measurements. *Chem. Commun.* **2019**, *55* (88), 13251–13254. https://doi.org/10.1039/c9cc06012j.

(7) Li, Y.; Wang, X.; Xu, D.; Chung, J. D.; Kaviany, M.; Huang, B. H2O Adsorption/Desorption in MOF-74: Ab Initio Molecular Dynamics and Experiments. *J. Phys. Chem. C* **2015**, *119* (23), 13021–13031. https://doi.org/10.1021/acs.jpcc.5b02069.

(8) Solovyeva, M. V.; Shkatulov, A. I.; Gordeeva, L. G.; Fedorova, E. A.; Krieger, T. A.; Aristov, Y. I. Water Vapor Adsorption on CAU-10- X: Effect of Functional Groups on Adsorption Equilibrium and Mechanisms. *Langmuir* **2021**, *37* (2), 693–702. https://doi.org/10.1021/acs.langmuir.0c02729.

(9) Tan, B.; Luo, Y.; Liang, X.; Wang, S.; Gao, X.; Zhang, Z.; Fang, Y. One-Pot Synthesis of Two-Linker Mixed Al-Based Metal-Organic Frameworks for Modulated Water Vapor Adsorption. *Cryst. Growth Des.* **2020**, *20* (10), 6565–6572. https://doi.org/10.1021/acs.cgd.0c00747.

(10) Rieth, A. J.; Hunter, K. M.; Dincă, M.; Paesani, F. Hydrogen Bonding Structure of Confined Water Templated by a Metal-Organic Framework with Open Metal Sites. *Nat. Commun.* **2019**, *10* (1), 1–7. https://doi.org/10.1038/s41467-019-12751-z.

(11) Hunter, K. M.; Wagner, J. C.; Kalaj, M.; Cohen, S. M.; Xiong, W.; Paesani, F. Simulation Meets Experiment: Unraveling the Properties of Water in Metal-Organic Frameworks through Vibrational Spectroscopy. *J. Phys. Chem. C* **2021**, *125* (22), 12451–12460. https://doi.org/10.1021/acs.jpcc.1c03145.

(12) Salles, F.; Bourrelly, S.; Jobic, H.; Devic, T.; Guillerm, V.; Llewellyn, P.; Serre, C.; Ferey, G.; Maurin, G. Molecular Insight into the Adsorption and Diffusion of Water in the Versatile Hydrophilic/Hydrophobic Flexible MIL-53(Cr) MOF. *J. Phys. Chem. C* **2011**, *115* (21), 10764–10776. https://doi.org/10.1021/jp202147m.

(13) Dietzel, P. D. C.; Johnsen, R. E.; Blom, R.; Fjellvåg, H. Structural Changes and Coordinatively Unsaturated Metal Atoms on Dehydration of Honeycomb Analogous Microporous Metal-Organic Frameworks. *Chem. - A Eur. J.* **2008**, *14* (8), 2389–2397. https://doi.org/10.1002/chem.200701370.

(14) Furukawa, H.; Gándara, F.; Zhang, Y. B.; Jiang, J.; Queen, W. L.; Hudson, M. R.; Yaghi, O. M. Water Adsorption in Porous Metal-Organic Frameworks and Related Materials. *J. Am. Chem. Soc.* **2014**, *136* (11), 4369–4381. https://doi.org/10.1021/ja500330a.

(15) Zhang, H.; Snurr, R. Q. Computational Study of Water Adsorption in the Hydrophobic Metal-Organic Framework ZIF-8: Adsorption Mechanism and Acceleration of the Simulations. *J. Phys. Chem. C* **2017**, *121* (43), 24000–24010. https://doi.org/10.1021/acs.jpcc.7b06405.

(16) Calero, S.; Gómez-Álvarez, P. Underlying Adsorption Mechanisms of Water in Hydrophobic and Hydrophilic Zeolite Imidazolate Frameworks: ZIF-71 and ZIF-90. *J. Phys. Chem. C* **2015**, *119* (41), 23774–23780. https://doi.org/10.1021/acs.jpcc.5b07360.

(17) Mileo, P. G. M.; Ho Cho, K.; Park, J.; Devautour-Vinot, S.; Chang, J. S.; Maurin, G. Unraveling the Water Adsorption Mechanism in the Mesoporous MIL-100(Fe) Metal-Organic Framework. *J. Phys. Chem. C* **2019**, *123* (37), 23014–23025. https://doi.org/10.1021/acs.jpcc.9b06228.

(18) Babin, V.; Leforestier, C.; Paesani, F. Development of a "First Principles" Water Potential with Flexible Monomers: Dimer Potential Energy Surface, VRT Spectrum, and Second Virial Coefficient. *J. Chem. Theory Comput.* **2013**, *9* (12), 5395–5403. https://doi.org/10.1021/ct400863t.

(19) Babin, V.; Medders, G. R.; Paesani, F. Development of a "First Principles" Water Potential with Flexible Monomers. II: Trimer Potential Energy Surface, Third Virial Coefficient, and Small Clusters. *J. Chem. Theory Comput.* **2014**, *10* (4), 1599–1607. https://doi.org/10.1021/ct500079y.

(20) Medders, G. R.; Babin, V.; Paesani, F. Development of a "First-Principles" Water Potential with Flexible Monomers. III. Liquid Phase Properties. *J. Chem. Theory Comput.* **2014**, *10* (8), 2906–2910. https://doi.org/10.1021/ct5004115.

(21) Dramstad, T. A.; Wu, Z.; Gretz, G. M.; Massari, A. M. Thin Films and Bulk Phases Conucleate at the Interfaces of Pentacene Thin Films. *J. Phys. Chem. C* **2021**, *125* (30), 16803–16809. https://doi.org/10.1021/acs.jpcc.1c04432.

(22) Neri, G.; Walsh, J. J.; Teobaldi, G.; Donaldson, P. M.; Cowan, A. J. Detection of Catalytic Intermediates at an Electrode Surface during Carbon Dioxide Reduction by an Earth-Abundant Catalyst. *Nat. Catal.* **2018**, *1* (12), 952–959. https://doi.org/10.1038/s41929-018-0169-3.

(23) Lu, H.; Huang, Y. C.; Hunger, J.; Gebauer, D.; Cölfen, H.; Bonn, M. Role of Water in CaCO3Biomineralization. *J. Am. Chem. Soc.* **2021**, *143* (4), 1758–1762. https://doi.org/10.1021/jacs.0c11976.

(24) Zhang, J.; Tan, J.; Pei, R.; Ye, S.; Luo, Y. Ordered Water Layer on the Macroscopically Hydrophobic Fluorinated Polymer Surface and Its Ultrafast Vibrational Dynamics. *J. Am. Chem. Soc.* **2021**. https://doi.org/10.1021/jacs.1c03581.

(25) Piontek, S. M.; Dellostritto, M.; Mandal, B.; Marshall, T.; Klein, M. L.; Borguet, E. Probing Heterogeneous Charge Distributions at the α-Al2O3(0001)/H2O Interface. *J. Am. Chem. Soc.* **2020**, *142* (28), 12096–12105. https://doi.org/10.1021/jacs.0c01366.

(26) Sudera, P.; Cyran, J. D.; Deiseroth, M.; Backus, E. H. G.; Bonn, M. Interfacial Vibrational Dynamics of Ice Ihand Liquid Water. *J. Am. Chem. Soc.* **2020**, *142* (28), 12005–12009. https://doi.org/10.1021/jacs.0c04526.

(27) Wang, C.; Zhang, T.; Lin, W. Rational Synthesis of Noncentrosymmetric Metal-Organic Frameworks for Second-Order Nonlinear Optics. *Chemical Reviews*. 2012, pp 1084–1104. https://doi.org/10.1021/cr200252n.

(28) McDermott, M. L.; Vanselous, H.; Corcelli, S. A.; Petersen, P. B. DNA's Chiral Spine of Hydration. *ACS Cent. Sci.* **2017**, *3* (7), 708–714. https://doi.org/10.1021/acscentsci.7b00100.

(29) Pullanchery, S.; Roke, S. Handy Water: Chiral Superstructures around Peptide β-Sheets. *Proc. Natl. Acad. Sci. U. S. A.* **2021**, *118* (2), 10–12. https://doi.org/10.1073/PNAS.2024376118.

(30) Wang, H.; Chen, W.; Wagner, J. C.; Xiong, W. Local Ordering of Lattice Self-Assembled SDS@2β-CD Materials and Adsorbed Water Revealed by Vibrational Sum Frequency Generation Microscope. *J. Phys. Chem. B* **2019**, *123* (29), 6212–6221. https://doi.org/10.1021/acs.jpcb.9b04928.

(31) Wang, H.; Wagner, J. C.; Chen, W.; Wang, C.; Xiong, W. Spatially Dependent H-Bond Dynamics at Interfaces of Water/Biomimetic Self-Assembled Lattice Materials. *Proc. Natl. Acad. Sci. U. S. A.* **2020**, *117* (38), 23385–23392. https://doi.org/10.1073/pnas.2001861117.

(32) Wang, H.; Xiong, W. Vibrational Sum-Frequency Generation Hyperspectral Microscopy for Molecular Self-Assembled Systems. *Annu. Rev. Phys. Chem.* **2020**, *72*, 279–306. https://doi.org/10.1146/annurev-physchem-090519-050510.

(33) Doughty, B.; Rao, Y.; Kazer, S. W.; Kwok, S. J. J.; Turro, N. J.; Eisenthal, K. B. Probing the Relative Orientation of Molecules Bound to DNA through Controlled Interference Using Second-Harmonic Generation. *Proc. Natl. Acad. Sci.* **2013**, *110* (15), 5756–5758. https://doi.org/10.1073/PNAS.1302554110.

(34) Rodriguez, D.; Marquez, M. D.; Zenasni, O.; Han, L. T.; Baldelli, S.; Lee, T. R. Surface Dipoles Induce Uniform Orientation in Contacting Polar Liquids. *Chem. Mater.* **2020**, *32* (18), 7832–7841. https://doi.org/10.1021/acs.chemmater.0c02471.

(35) Wang, H.; Gao, T.; Xiong, W. Self-Phase-Stabilized Heterodyne Vibrational Sum Frequency Generation Microscopy. *ACS Photonics* **2017**, *4* (7), 1839–1845. https://doi.org/10.1021/acsphotonics.7b00411.

(36) Wang, H.; Gao, T.; Xiong, W. Self-Phase-Stabilized Heterodyne Vibrational Sum Frequency Generation Microscopy. *ACS Photonics* **2017**, *4* (7), 1839–1845. https://doi.org/10.1021/acsphotonics.7b00411.

(37) G. Nicolau, B.; García-Rey, N.; Dryzhakov, B.; D. Dlott, D. Interfacial Processes of a Model Lithium Ion Battery Anode Observed, in Situ, with Vibrational Sum-Frequency Generation Spectroscopy. *J. Phys. Chem. C* **2015**, *119* (19), 10227–10233. https://doi.org/10.1021/acs.jpcc.5b01290.

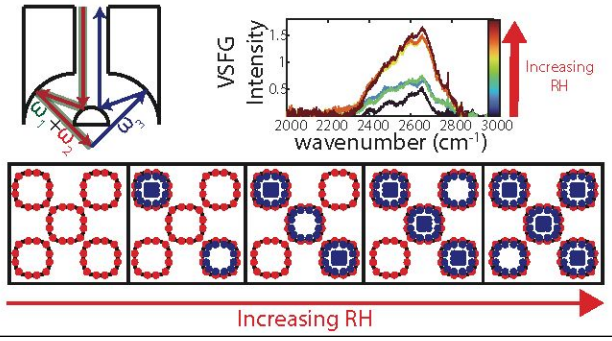

For Table of Contents Only